OpenFOAM Finite Volume Method Implementation of a Fully Nonlinear Potential Flow Model for Simulating Wave-Structure Interactions

Graham, DI; Mehmood, A; langfeld, K; greaves, D

Published in:
Proceedings of the Twenty-fifth (2015) International Ocean and Polar Engineering Conference

Publication date:
2015

OpenFOAM Finite Volume Method Implementation of a Fully Nonlinear Potential Flow Model for Simulating Wave-Structure Interactions

Arshad Mehmood [a,*], *David I. Graham* [a], *Kurt Langfeld* [a], *and Deborah M. Greaves* [b]

[a] School of Computing and Mathematics, Plymouth University, Plymouth, UK
[b] School of Marine Science and Engineering, Plymouth University, Plymouth, UK

ABSTRACT

We develop an interface-tracking algorithm to solve the two-dimensional time dependent free surface flows using a finite volume method with full nonlinear free surface boundary conditions and moving grids. The velocity potential is obtained inside the fluid domain by solving a mixed boundary value problem. The velocity is then calculated by the gradient of the velocity potential. The motion of the free surface is captured by integrating in time the kinematic boundary condition, which is based on the free surface volume flux. In the implemented scheme, the free surface is allowed to deform and a new mesh is generated at each time step. The basis of this model is the freely available open-source computational fluid dynamic toolbox OpenFOAM®). We examine the spatial and temporal convergence of the scheme. We also compare wave periods and evolution of wave amplitudes for a range of wave conditions with the analytical solutions, and a good agreement is found. The solver is intended to be a first step towards an advanced numerical wave tank solving both incompressible and compressible flows interacting with structures undergoing large body motions.

KEY WORDS: Finite volume method; nonlinear full potential flow solver; dynamic mesh; interface-tracking algorithm.

1 INTRODUCTION

Numerical modeling of free surface water waves typically uses two distinct approaches namely "surface capturing" (Jacobsen et al. (2011)) and "surface tracking" (Greaves et al. (1997); Wu and Taylor (1994); Ma et al. (2001*a*); Santos and Greaves (2007)). Surface capturing approaches include "volume of fluid" and "level set" methods. In these methods a scalar function is used to determine the location of the interface between the two fluids (air and water). The scalar function is traced by solving an additional scalar transport equation. The advantages of these methods include modeling of complex flow phenomena such as wave breaking, overtopping, and cavitation without any further modifications to the base algorithm. However, the interface between the two fluids is not precise (Floryan and Rasmussen (1989)), since the scalar field diffuses close to the interface. Moreover this approach also requires the solution of at least two fluids resulting in higher computational cost. On the other hand surface tracking methods (Greaves et al. (1997); Wu and Taylor (1994); Ma et al. (2001*a*); Santos and Greaves (2007)) are generally based on boundary-fitted grids that move and deform as the solution advances in time. The advantages of this approach includes accurately determining the free surface profile and moreover this approach requires the solution of only one fluid resulting in low computational cost.

Both these approaches are further subdivided into two: Navier-Stokes or Euler equations solutions; or the hypothesis of irrotational flow leading to potential flow solutions. Significant progress has been made employing both scenarios in order to explore the physics of various kinds of waves. Mayer et al. (1998) and Muzaferija and Peric (2007) numerically captured the nonlinear free surface waves for full flow conditions using the finite volume method. The governing field equations were the incompressible Navier-Stokes equations. The position and shape of the free surface was determined by integrating the kinematic boundary condition. A detailed review about the developments for the modeling moving boundary problems for the Navier-Stokes equations was given by Floryan and Rasmussen (1989). They discussed the base methods like Eulerian, Lagrangian, and mixed (Eulerian-Lagrangian). Moreover, they also analysed utilization of

*arshad.mehmood@plymouth.ac.uk

moving grids, adaptive grids, grids of variable topology and connectivity.

For an irrotational flow, various methods have been applied to capture the free surface profile accurately and with less computational cost. Wu and Taylor (1994) numerically simulated two-dimensional free surface waves using two different finite element approaches. In the first one, velocity potential was considered as the only unknown, and in the second both the velocity potential and the flow velocities were treated as unknowns and were solved together. Ma et al. (2001a) developed a numerical methodology also using the finite element technique to capture the three dimensional interaction between waves and stationary rigid bodies. They also applied a recovery technique to improve the accuracy of the solution without additional computational cost. They developed a radiation condition which was based on the combination of a damping zone and the Sommerfeld condition, to minimize effectively the effect of the reflected waves from the rigid boundaries. Santos and Greaves (2007) using a finite difference method captured the irrotational nonlinear free surface water waves. They applied the Lagrangian-Eulerian approach where the interior of the fluid domain was discretized using an Eulerian quadtree grid, whilst the free surface was tracked using a Lagrangian approach. The coupling between the Lagrangian particles on the free surface and the interior of the fluid domain was achieved by computing the normal and tangential components of the free surface velocities.

In this paper, following the irrotational flow assumption, we describe a moving boundary finite volume formulation for two-dimensional fully nonlinear time-dependent free surface waves. The governing equation is Laplace's equation written in terms of the velocity potential. We apply Neumann type boundary conditions on rigid boundaries and kinematic and dynamic boundary conditions on the free surface. In the implemented scheme, the free surface is allowed to deform and a new mesh is created at each time step. The basis of this model is the freely available open-source computational fluid dynamic toolbox OpenFoam®, which is distributed by OpenCFD®. However, modeling of the nonlinear free surface waves which satisfies the Laplace's of the velocity potential inside the fluid domain with the inclusion of kinematic and dynamic boundary conditions were not part of the standard distribution. OpenFOAM® uses a finite volume discretisation approach on unstructured meshes consisting of arbitrary convex polyhedrals. For a full description of space and time integration schemes in OpenFOAM®, readers are referred to (Jasak (1996)). The paper is organized as follows. In Section 2, we discuss the mathematical formulation of the scheme. In Section 3, we discuss the obtained numerical results. Conclusions are presented in Section 4.

2 MATHEMATICAL FORMULATION

The flow is assumed to be incompressible, inviscid, and irrotational. The governing equation of the fluid flow is given by:

$$\nabla^2\phi = 0, \tag{1}$$

where ϕ represents the velocity potential. A Cartesian coordinate system is employed to simulate the flow field with y directed vertically upward and the origin located at the mean water level as shown in Fig. 1. All the field variables are defined at cell centres. We compute the fluid velocities by its gradient, $u = \nabla\phi$. On all rigid surfaces, the Neumann type boundary condition is applied. At the free surface, the dynamic and the kinematic boundary conditions are imposed and are given as:

$$\frac{\partial\phi}{\partial t} = -g\zeta - \frac{1}{2}\nabla\phi.\nabla\phi, \tag{2}$$

$$\frac{\partial\zeta}{\partial t} = \frac{\partial\phi}{\partial y} - \frac{\partial\phi}{\partial x}\frac{\partial\zeta}{\partial x}, \tag{3}$$

where ζ is the free surface position, g is the acceleration due to gravity, ∇ is the gradient operator vector and t is time. The kinematic boundary condition based on the volume flux can be written as (Mayer et al. (1998),

$$\frac{\partial\zeta}{\partial t} = \frac{\mathbf{U_f}}{dA}.n, \tag{4}$$

where $\mathbf{U_f}$ is the volume flux, dA is the cell face area and n is the unit normal out of the flow domain.

Eq. 4 expresses the temporal change of the free-surface geometry based on the volume flux. The mesh is updated based on the new position of the free surface geometry. Then Eq. 2 is evaluated to give the updated velocity potential for the next time step. Note that in OpenFOAM, the flow variables are defined at the cell centre and the fluxes are computed at the face centres. Moreover, the boundary conditions are defined at the face centre. However, the free-surface geometry must be specified at cell vertex points when used for the grid generation. Therefore, we interpolate the flux values from the face centre to the cell vertices and integrate the values according to Eq. 4. Moreover, to apply the dynamic boundary condition, we interpolate back the cell displacement ζ to the face

centre. Furthermore, the velocities are not defined at cell face boundaries, they are only defined at cell centres, we therefore extrapolate the velocities using first-order extrapolation to the face centre. The dynamic boundary condition is then solved to give the velocity potential on the free surface for the next time step.

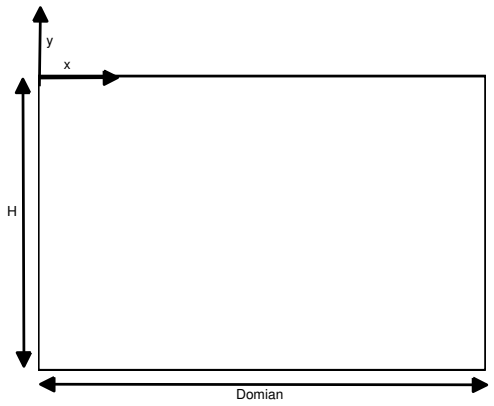

Fig. 1 A 2-D layout of the domain.

2.1 Sequence of Solution Procedure

The sequence followed for integrating the system of fluid motion and free surface from time step t^n to t^{n+1} is as follows.

1. Generate the grid.
2. Read/create all the fields (e.g velocity potential and surface elevation ζ).
3. Apply the boundary conditions.
4. Solve Laplace's equation for the velocity potential ϕ.
5. Compute the required variables (i.e, velocities $\mathbf{u_i}$, fluxes $\mathbf{U_f}$).
6. Solve the kinematic boundary condition using Eq. 4, yielding new free surface geometry.
7. Update the grid based on the surface elevation computed in the previous step (step 6).
8. Compute the dynamic boundary condition using Eq. 2.
9. Repeat the procedure (step 4-8) to march in time.

3 RESULTS and DISCUSSION

3.1 Spatial and Temporal Convergence

We consider various cases of standing waves and compare the numerical simulation results with the analytical solution. The standing waves are generated by setting the initial shape of the free surface defined by a sinusoidal function, $\zeta = a\sin(kx)$ where k is the wave number and x is measured along the length of the tank (Santos and Greaves (2007)) as shown in Fig. 2. We use a Crank-Nicolson method for the time integration of the kinematic and dynamic boundary conditions in all the simulations. For grid convergence, we simulated a sinsoidal wave of amplitude $a = 0.01$ m, wavelength $\lambda = 1.0$ m and a mean water depth of $H = 0.8$ m on a series of regular grids as tabulated in table 1 using a dimensional time step $\Delta t = 0.005$ s. The error is plotted against the number of grid points along the x-direction on a log log scale as shown in Fig. 3. The error is calcuated from the absolute difference between the analytical solutions and the calculated values of wave elevation measured at the centre of the domain. We note from this plot that error decreases as the number of grid points are increased; showing first order accuracy as expected. To optimize the simulations in terms of the computational cost, Grid-4 is used with $\Delta t = 0.005$ s for the remaining simulations, unless stated otherwise.

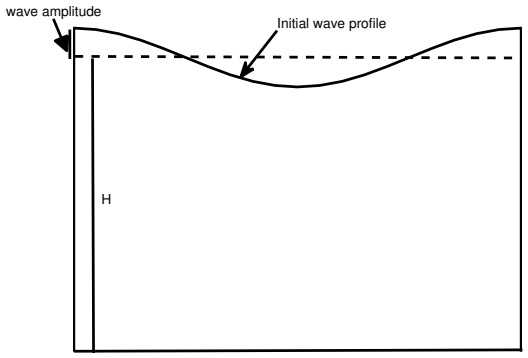

Fig. 2 Initial profile of the standing wave.

We also carried out the time discretisation study. For that purpose we consider Grid-4 having 49 grid points along the x-direction and 39 grid points along the y-direction. A sinosoidal wave of amplitude a=0.01 m,

Table 1 Mesh details and the error calculated.

Cases	Grid size
Grid-1	13 x 11 x 1
Grid-2	20 x 17 x 1
Grid-3	33 x 26 x 1
Grid-4	49 x 39 x 1
Grid-5	75 x 59 x 1
Grid-6	113 x 89 x 1
Grid-7	169 x 134 x 1
Grid-8	211 x 167 x 1
Grid-9	253 x 201 x 1

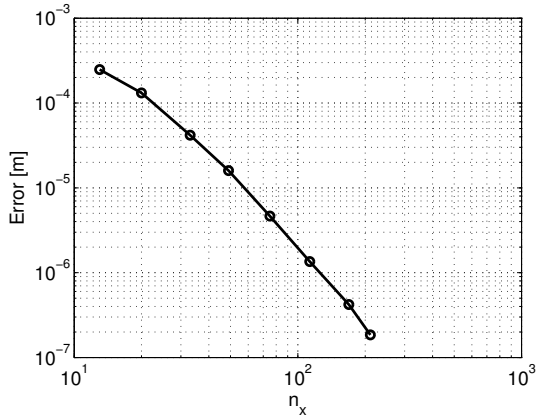

Fig. 3 Calculated error vs number of grid points along x-direction.

$\lambda = 1.0$ m was simulated. The mean water depth was set to H=0.8 m. The simulations were carried out for time steps $\Delta t = 0.025$, $\Delta t = 0.0125$, $\Delta t = 0.00625$, $\Delta t = 0.003125$. Fig. 4 shows the L_1-error against the time steps. This plot shows the decrease in error with the decrease in time step size; showing satisfactory temporal convergence.

3.2 Wave Period Comparison

In this section, we compare the wave period obtained for different cases ranging from shallow water to deep water and compare with the wave period obtained from 2nd-order Airy wave theory. We consider two different wave amplitudes $a = 0.005$ m and 0.01 m where the wavelength is set to $\lambda = 1.0$ m. We vary the mean water depth with small increments. The obtained wave periods from the current simulations are plotted against the mean water depth as shown in Fig. 5 along with the analytical values. The numerical wave period was obtained from the difference of the first two consecutive crests of the wave

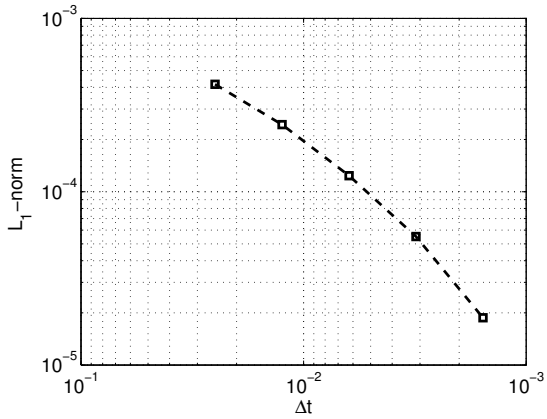

Fig. 4 variation of error estime with time step Δt.

elevation time trace. The analytical wave period based on 2nd-order Airy wave theory was calculated according to the dispersion relation $T = \frac{2*\pi}{\sqrt{((g*k*tanh(k*H)))}}$ where k is the wave number and g is the gravitational acceleration. This plot shows that the obtained wave period from the current numerical scheme agrees very well to that predicted by 2nd order Airy wave theory.

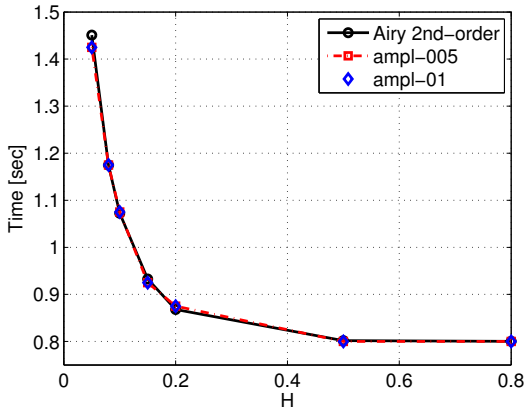

Fig. 5 Variation of wave period against mean water depth normalized by wavelength λ.

3.3 Small and Large Amplitude Waves Comparison with Analytical Solutions

In this section, we compare the time history of the wave elevation with the analytical solutions for low and relatively large amplitudes. Firstly, we simulated low ampli-

tude waves where the effect of nonlinear terms appearing in the dynamic boundary condition can be neglected. As a result, the simulation results can be compared with those predicted by linear anlaytical solutions. For that purpose, we consider standing sinusoidal waves with amplitudes $a = 0.005$ m and $a = 0.01$ m, wavelength $\lambda = 1$ m and mean water depth $H = 0.8$ m. The time traces of the free surface elevation calculated at the centre of the tank for both wave amplitudes are shown in Fig. 6. This plot shows good agreement with the linear analytical solution for both amplitudes. The calculated error for wave amplitudes $a = 0.01$ m only is also plotted as shown in Fig. 7 . Qualitatively the same pattern of the error was found for wave amplitude $a = 0.005$ m. It can be noted from this plot that error grows with time. In fact the error growth is purely due to the difference between the frequency of the analytical solution and that found in the numerical solution. We note that the wave amplitude is well predicted, and when we multiply the wave frequency with a factor very close to 1, in this particular case the factor was 0.998, the error does not grow and remians very low as shown by black solid line in Fig. 7. It is important to note that this phase difference reduces as the grid is refined.

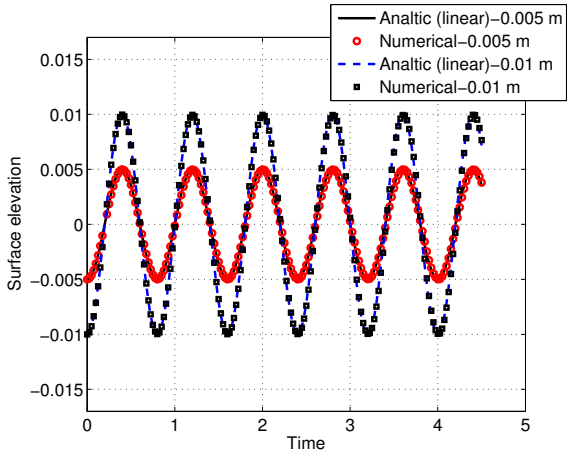

Fig. 6 Time history of free surface elevation at the centre of the domain where $H = 0.8$ m and $\lambda = 1$ m.

We also compare the results obtained for a relatively large amplitude. As the wave amplitude increases, the velocities at the free surface appearing in the boundary conditions become significant. Since their product brings nonlinearity to the solution, their accurate calculation is necessary. Moreover, the velocities are not computed at the free surface but they are interpolated from the cell centre. We need a much finer grid close to the free surface. For that purpose, we use a graded grid of Grid-

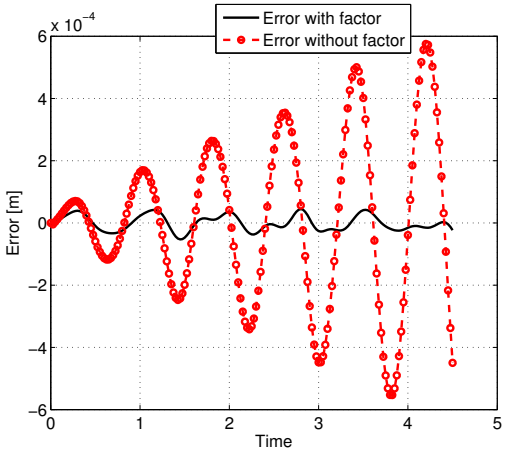

Fig. 7 Time history of the error when $a = 0.01$ m, $H = 0.8$ m and $\lambda = 1$ m.

4 which make a finer grid close to the free surface and a comparatively coarser grid away from the free surface without adding any computational expense. We consider a standing sinusoidal wave with amplitudes $a = 0.03$ m, wavelength $\lambda = 1$ m and mean water depth $H = 0.8$ m. The time trace of the wave elevation measured at the centre of the domain is shown in Fig. 8. The 2nd-order Airy solution was plotted based on the following relation Cozzi (2010)

$$\begin{aligned}\zeta(x,t) =& a\cos(kx)\cos(\omega t)+ \\ & \frac{\pi a^2}{\lambda}[\cos^2(\omega t) - \frac{1}{4\cosh^2(kH)}+ \\ & \frac{3}{4\sinh^2(kH)}\cos(2\omega t)]\cos(2kx), \end{aligned} \quad (5)$$

This plot shows qualitatively good agreement with the 2nd-order Airy wave solution and also showing sharper crests and higher harmonics, the phenomenon also observed by (Ma et al. (2001*b*); Santos and Greaves (2007)).

The current nonlinear full potential flow (NLFP) solver has been developed in OpenFOAM environment. Possible advantages include utilization of their built-in utilities including parallelization, various time and spatial discretisation schemes, meshing types, mesh motion solvers, selection of different waves. Moreover, OpenFOAM has already built-in incompressible and compressible Navier-Stokes (NS) solvers where the ultimate goal is to couple the NLFP with incompressible and compressible NS solvers through a proper boundary condition that will enable simulations of the full range of wave conditions.

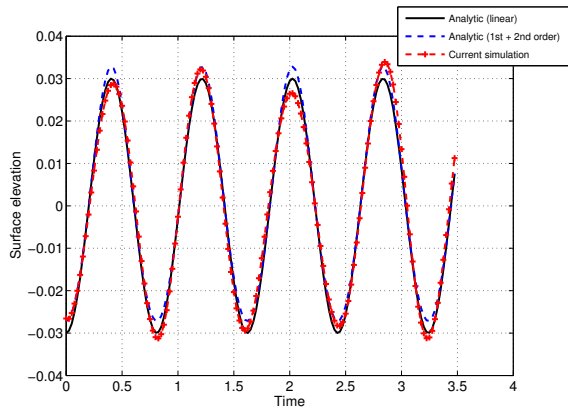

Fig. 8 Time history of free surface elevation at the centre of the domain where $a = 0.03$ m, $H = 0.8$ m and $\lambda = 1$ m.

4 CONCLUSIONS

The two-dimensional nonlinear transient free surface flow problem has been solved using the finite volume method. The method have been used to simulate various kinds of standing waves in a rectangular tank. We have found good spatial and temporal convergence of the solver. Also, the wave period as predicted by 2nd-order Airy wave theory for a range of scenarios ranging from shallow water to deep water was well captured by the current scheme. Excellent agreement with the analytical solutions for different wave amplitudes show successful implementation of the kinematic and dynamic boundary conditions in the OpenFOAM. The success of the method suggests that this approach can be easily extended to three-dimensional nonlinear free surface waves.

The developed solver and the associated kinematic and dynamic boundary conditions will be released as an open-source for the marine and offshore community.

ACKNOWLEDGEMENT

The author gratefully acknowledge the EPSRC grant reference number EP/K038303/1 for the financial support for the current work.

References

Cozzi, O. (2010), Free surface flow simulation correcting and benchmarking the ALE method in Code_Saturne, PhD thesis, The University of Manchester.

Floryan, J. and Rasmussen, H. (1989), 'Numerical methods for viscous flows with moving boundaries', *Applied Mechanics Reviews* **42**(12), 323–341.

Greaves, D., Borthwick, A., Wu, G. and Taylor, R. (1997), 'A moving boundary finite element method for fully nonlinear wave simulations', *Journal of Ship Research* **41**(3), 181–194.

Jacobsen, N., Fuhrman, D. and Fredsoe, J. (2011), 'A wave generation toolbox for the open-source cfd library: Openfoam', *International Journal for Numerical Methods in Fluids* **70**(2), 181–194.

Jasak, H. (1996), Error analysis and estimation for the finite volume method with applications to fluid flows, PhD thesis, Imperial College of Science, Technology and Medicine.

Ma, Q., Wu, G. and Taylor, R. (2001*a*), 'Finite element simulation of fully non-linear interaction between vertical cylinders and steep waves. part 1: Methodology and numerical procedure', *International Journal for Numerical Methods in Fluids* **36**, 265–285.

Ma, Q., Wu, G. and Taylor, R. (2001*b*), 'Finite element simulation of fully non-linear interaction between vertical cylinders and steep waves. part 2: Numerical results and validation', *International Journal for Numerical Methods in Fluids* **36**, 287–308.

Mayer, S., Garapon, A. and Sorensen, L. (1998), 'A fractional step method for unsteady free-surface flow with applications to non-linear wave dynamics', **28**, 293–315.

Muzaferija, S. and Peric, M. (2007), 'Computation of free-surface flows using the finite-volume method and moving grids," numerical heat transfer, part b: Fundamentals:', *International Journal of Computational Methods* pp. 369–384.

Santos, C. and Greaves, D. (2007), 'A mixed lagrangian-eulerian method for non-linear free surface flows using multigrid on hierarchical cartesian grids', *Computer & Fluids* **36**, 914–923.

Wu, G. and Taylor, R. (1994), 'Finite element analysis of two-dimensional non-linear transient water waves', *Applied Ocean Research* **16**, 363–372.